

A single slotted morphing flap based on SMA technology

Salvatore Ameduri^{*1}, Antonio Concilio^{1a}, Rosario Pecora^{2b} and
Dimitrios Karagiannis^{3c}

¹Department of Adaptive Structures, Centro Italiano Ricerche Aerospaziali,
Via Majorise, 81043, Capua (CE), Italy

²Department of Aerospace Engineering, Università degli Studi di Napoli "Federico II",
Via Claudio, 21, 80125, Napoli, Italy

³INASCO Hellas Co, Napoleontos Zerva 18, 16675, Glifada, Greece

(Received March 12, 2014, Revised November 21, 2015, Accepted March 7, 2016)

Abstract. In this paper, the activities carried out within the EU funded Clean Sky Joint Technology Initiative (JTI GRA) Project and aimed at developing a morphing flap, are illustrated. The reference device is a regional aircraft single slotted flap, enhanced with deforming capabilities to obtain improved hyper-lift performance. The design started with the identification of the internal architecture, intended to allow camber variations. A concentrated-hinge architecture was selected, for its ability to fit different curvatures and for the possibility of easily realizing an "armadillo-like" configuration, then avoiding the use of a complicate deformable skin. The flap layout is made of segmented ribs, elastically hinged each other and span-wise connected by conventional spars. Relative rotations of the rib elements are forced by SMA structural actuators, i.e., cooperating in the external loads absorption. Super-elastic SMA are used to make up recovery elastic elements, necessary to regain the original shape after activation. These further elements in turn contribute to the overall flap rigidity. After assessing the hinge number and the size of the SMA active and passive elements, the advanced design phase was dealt with. It was aimed at solving manufacturing issues and producing the executive drawings. The realized demonstrator was finally tested in lab conditions to prove its functionality in terms of whether target shape actuation or attained shape preservation under loads. On the basis of the numerical results and the experimental outcomes, precious hints were obtained for further developments of the concept.

Keywords: shape memory alloys; smart structures; morphing; flap

1. Introduction

Adaptive variation of aerodynamic surfaces geometry (morphing) discloses wide potentialities for aircraft design. Expected benefits involve in principle the entire flight envelope, assuming the capability to attain the optimal configuration for each flight regime, (Stanewsky 2001). Depending on the final targets, a number of parameters may be improved: aerodynamic efficiency (drag

*Corresponding author, Ph.D., E-mail: s.ameduri@cira.it

^a Ph.D., E-mail: a.concilio@cira.it

^b Ph.D., E-mail: rosario.pecora@unina.it

^c Ph.D., E-mail: d.karagiannis@inasco.com

reduction, L/D ratio increase, difference between the maximum dash speed and the minimum loiter speed (Lesieutre *et al.* 2011) etc.), maneuverability or stability levels (commands effectiveness, time response, etc.), environmental impact ratio (reduction of general emissions level, etc.), maintenance easiness (parts number reduction, simpler architectures, etc.), weight, cost and many others, (Stanewsky 2001, Lesieutre *et al.* 2011, Monner *et al.* 1998, Perkins *et al.* 2004).

The so-called smart materials, able to alter some of their physical or geometrical properties, offered additional design opportunities. Shape Memory Alloys (SMA) show peculiar strain recovery and super-elastic capacities. This performance transforms into an outstanding ability in producing large forces and displacements, while exhibiting significant mechanical properties (Moses 1997). They can make possible the realization of very compact actuators, demonstrating to be an absolute candidate for morphing structures, (Mcknight *et al.* 2010, Barbarino *et al.* 2007, Barbarino *et al.* 2009). More recent works demonstrate the possibility of using these materials to control the achieved morphed geometry (Bil *et al.* 2013, Grigorie *et al.* 2011a, b).

Morphing is based on the main assumption that the shape changing architecture must also absorb the external loads. This requires a structure both rigid and deformable. The authors achieved these antithetic objectives by using load-bearing actuation systems (Iannuzzo *et al.* 2009). The wide interest in the morphing approach led to dedicated investigations and research programs aimed at increasing the technology readiness of these novel approaches for finally arriving to viable industrial products. Among the others, one recalls: the DARPA/AFRL/NASA Smart Wing program (1995-2001), focusing on the development of smart technologies and demonstration of relevant concepts to improve the aerodynamic performance of military aircrafts (Kudva 2001, Inman 2011); the “Active aeroelastic aircraft structures (3AS)” (2002-2005) (Schweiger *et al.* 2002, Ameduri *et al.* 2009), with the overall objective of developing and evaluating adaptive stiffness concepts to improve aircraft efficiency through the exploitation of airframe aeroelastic deformations; the “Smart High Lift Devices for Next Generation Wings (SADE)” European Frame (2008-2012), (Guo 2012, SADE website), addressing the development and testing of novel morphing architectures for high lift performance and to preserve at the same time the laminar flow; the “Smart Intelligent Aircraft Structures (SARISTU)” European Project, focusing on the cost reduction of air travel through a variety of individual morphing applications as well as their combination (Dimino and Concilio 2013).

In this paper, the activities performed within the Clean Sky Joint Technology Initiative (JTI) are presented, focusing on the development of a shape-adaptive flap segment to enhance the capabilities of standard hyper-lift generators, (Call SP1-JTI-CS-2011-1-GRA-02-015, website 2011). The main target of the Clean Sky Program is the development of sustainable and breakthrough technologies such as new materials, aerodynamic models, environmentally friendly turbines, intelligent Life Cycle Assessment Tools to significantly improve the impact of the air transport on the environment.

At first, the internal architecture was identified. Among the candidates, classical ribs were substituted by finger-like structures, selected for their ability to fit shapes characterized by different cambers and the possibility of avoiding the use of specific skins by implementing armadillo-like configurations (sliding surfaces). The relative rotation of the rib elements was obtained by SMA-based actuators, cooperating in bearing the aerodynamic loads. Because elastic elements are necessary to regain the initial position, an extra rigidity is further added to the morphing flap (Ameduri *et al.* 2011a, b, Brindisi *et al.* 2011, Pecora *et al.* 2011).

Device sizing was then dealt with. The number of hinges was fixed as a compromise among the capability to fit the target shape, the constructive simplicity and the available room. SMA active

elements and spring recovery components were dimensioned by implementing a multi-objective optimization approach. Parameters like actuator authority, load-bearing capabilities; structural and SMA stress levels, weight, were taken into account. Their value was then frozen at the end of this step and used as input for the advanced design phase.

In the successive step, constructive details were set. Practical aspects like the connection of the SMA elements to the structure, the heating architecture (aimed at the minimum interference with the surrounding system), hinges mounting details, rib parts connections were solved in this phase. A flap prototype and a dedicated test rig were in the end manufactured to undergo static and dynamic tests. Both laser and strain gages were used to measure displacements and deformations in both reference and actuated configurations, either loaded or not. In the static campaign, the prototype proved to modify and maintain its shape under the most severe design load condition.

Accelerometers were used to detect the dynamic deformed shape. Eigen-frequencies resulted far away from the flap working range, so giving some hints on its aero-elastic robustness. SMA activation did not cause any significant variation. Experimental results were eventually compared with the numerical predictions and proved the functionality of the concept.

2. Specifications and selected architecture

The complete reference device is a single slotted flap, able to translate downward when rotating clockwise (lift enhancer). Morphing capabilities were supposed to increase the hyper-lift generation performance while leaving unaffected its standard way of working. A schematic of the airfoil integrated with the flap in morphed-optimised and unmorphed configuration is illustrated in Fig. 1.

Aerodynamic investigations identified the target morphed geometry, Fig. 2, able to meet specified performance targets, (Di Muzio 2010). The main advantage expected is in terms of the maximum lift from an initial value of 3.3 to 3.4 for an angle of attack of 5 deg. Mean line curvatures and angles are coincident up to the 20% of the flap chord (4% if referred to the main airfoil), in respect of design specs (fore part should have been rigid, red zone in Fig. 2). This segment is in fact the one demanded to host the flap kinematic system.

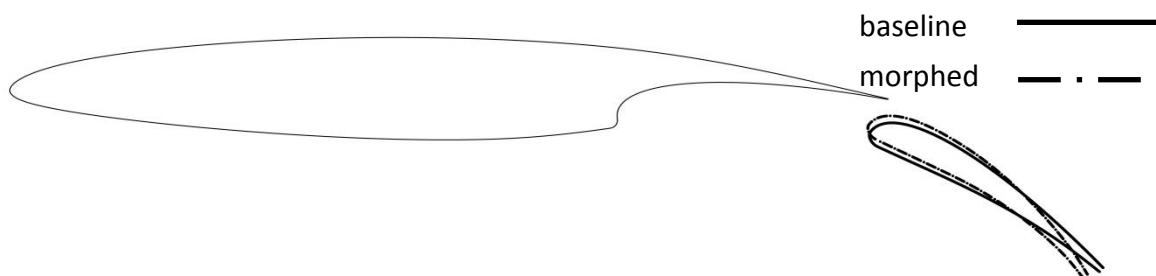


Fig. 1 Airfoil integrated with the flap in morphed-optimised (dashed) and unmorphed (solid) configuration

The morphing system shall assure the achievement of the specified shape under the external load action and the preservation of the structural integrity (geometrical and physical requirements). Unloaded morphing can be met by considering an adequate number of degrees of freedom, like a sufficient number of hinges along the mean chord. This number should however be kept low to limit the system complexity. To hold the deformed shape under the action of external forces instead, a certain stiffness level shall be guaranteed. SMA and added elastic recovery elements may be then properly sized in order to satisfy this need. Structural integrity is finally warranted by considering suitable constraints in the optimization design process. A significant simplification follows the intrinsic nature of the selected “armadillo” architecture (sliding rib parts), Fig. 3.

Because of the segmented architecture, the curvature variation of the investigated morphing flap is concentrated only at certain zones of the chord, i.e. the connection hinges. The aerodynamic performance is preserved by a proper design of the rotational path of each box with respect to its next, avoiding gaps and discontinuities as much as possible. In this configuration, hinges play a fundamental role: their bending stiffness strongly affects the over-all flap rigidity and the actuation performance. Pre-design is thus aimed at defining the hinges rigidity and the actuators features.

The actuation system uses SMA active elements. They can give rise to large displacements and transmitted forces; they are compact and easily embeddable into a generic structure. Therefore, they are very good candidates for the presented application. SMA wires were selected, intended sufficient to the proposed aims and able to guarantee a significant reduction of activation times and power. After activation, the actuator needs an elastic recovery element to recuperate its initial shape. Its rigidity is added to the structural stiffness to make the global resistance the SMA device shall overcome during actuation. Their design shall then take into account the two conflicting requisites of assuring the recovery and not hindering SMA actuation. Finally, combined SMA and elastic elements stiffness shall counteract the external loads in order to preserve the target shape.

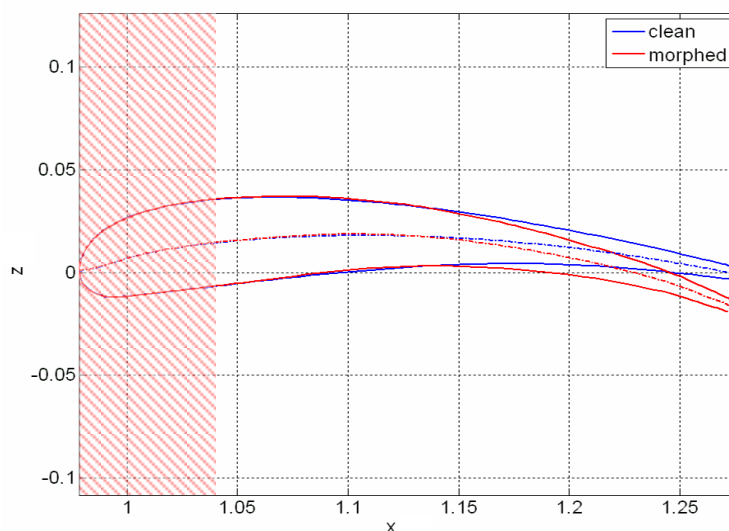


Fig. 2 Clean and morphed flap shapes; dimensionless data (reference: airfoil chord).

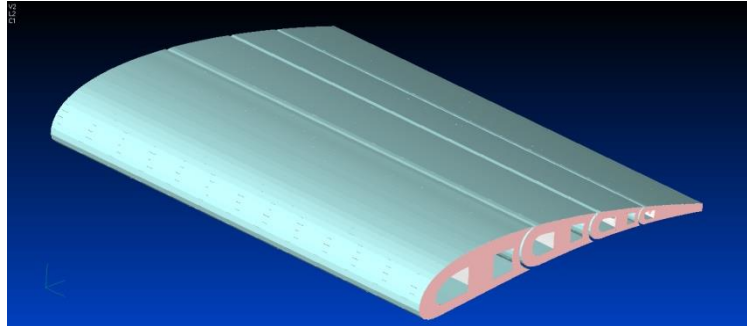


Fig. 3 Structural lay-out of the morphing flap

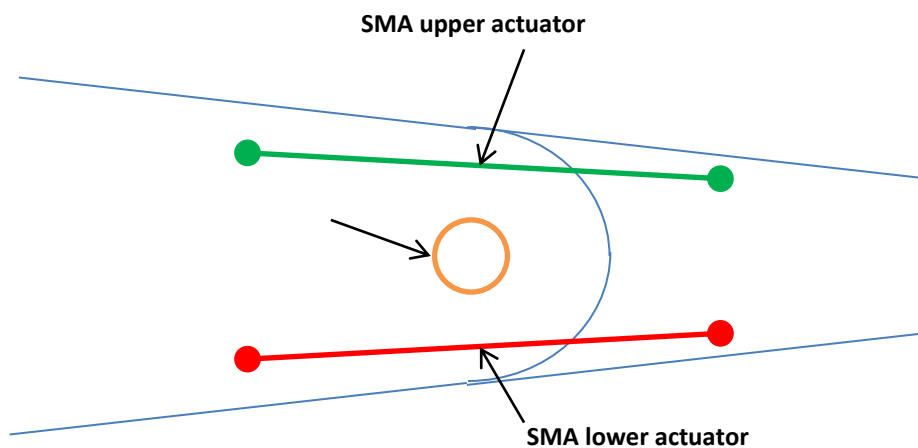


Fig. 4 SMA elements mounted in antagonistic configuration: actuator (red), elastic recovery element (green)

In the reported case, SMA was selected for the elastic recovery elements. In this case, super-elastic property is exploited: in fact, this material has the uncommon ability to afford large excursions without compromising its integrity and assuring a complete recovery when the load is removed (Langbein 2012). Resulting lay-out is an antagonistic configuration, Fig. 4, where the active (contracting) elements are located under the hinges, while the elastic recovery elements are on the top. A 3-hinge rib layout was selected, considered a good compromise between the ability of fitting the target shape and the system complexity.

3. Preliminary design

The flowchart illustrated in Fig. 5 defines the preliminary design path of the SMA passive (super-elastic) element. The same scheme maybe however exploited with some minimal difference to the SMA active component. The design is aimed at defining the specific physical and geometrical features (cross section area, length, material, pivot distance). Different robustness

criteria are implemented, on a step-by-step basis. First buckling verification of the elastic structure is performed under the most severe external loads. If no buckling occurs, necessary elastic pre-stress is computed, able to guarantee the full recovery after activation and following relaxation (i.e., the activation is over). If the structural stress level is again lower than the buckling limit, structural stress levels are verified to be under the allowable threshold (combined pre-stress and external loads action). The elastic element is then considered valid and the geometry and stress field parameters are held for next evaluations.

This scheme was then used as a flow-diagram of a genetic algorithm aimed at minimizing the deviation of the actual with respect to the target deflection at the hinge station (Maheri and Isikveren 2011). Design parameters were the cross section area, the length and the distance from the hinge of both the active and the antagonistic elements. Such values were weighted with respect to achieved stress levels, maximum attainable rotation, resulting structural system stiffness, required activation energy and total mass. The process was repeated for 20 different initial set of outline (populations), each made of 50 layouts (individuals). At the end of the optimizations, in fact, 20 sub-optimal solutions were identified. Their different performances were compared through radar diagrams, in order to select the best outline. The same logic was followed for each of the three hinges, the chosen architecture referred to.

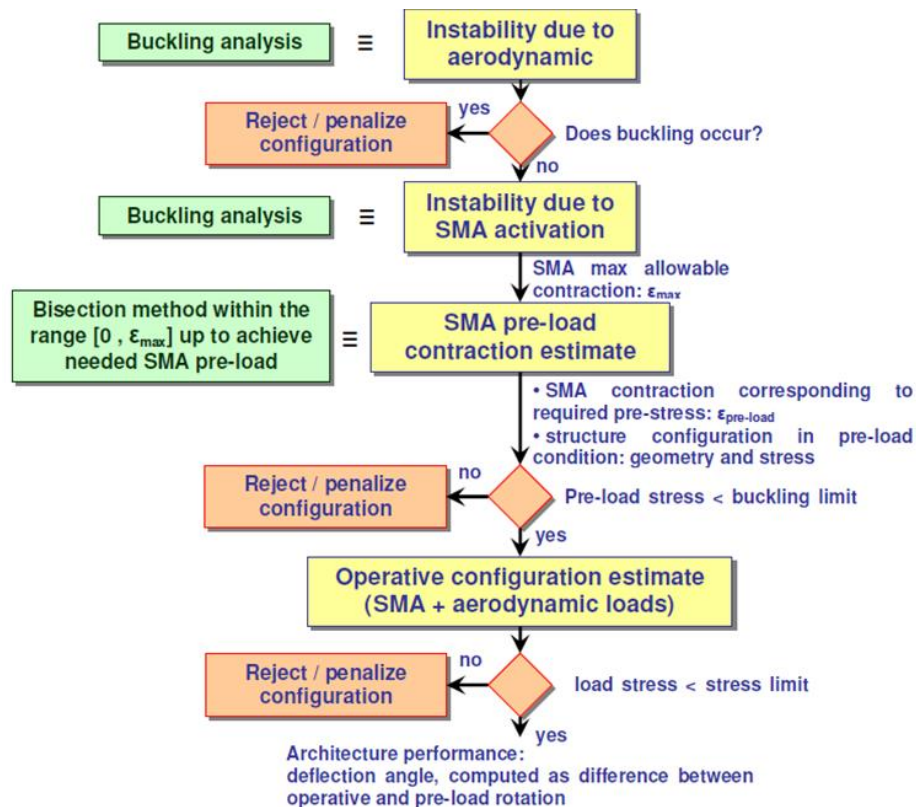


Fig. 5 SMA actuators mounted in antagonistic configuration

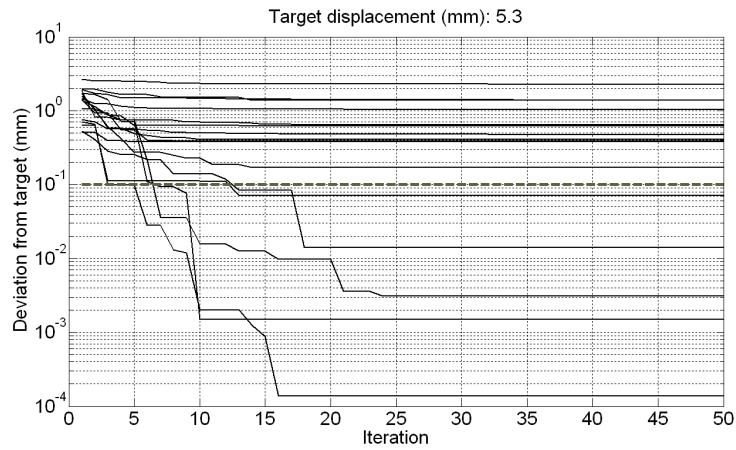


Fig. 6 Fitness value and convergence for a hinge

As reference scheme of the flap the drawings of Fig. 8 were adopted.

The convergence history and a radar diagram example are reported in Figs. 6 and 7, respectively. The dashed line in Fig. 6 represents the fixed threshold of 0.1 mm on the geometrical deviation: solutions exhibiting values over that line were discharged. The terms *MS_sig*, *MS_aero*, *MS_W*, *MS_SMA* and *MS_buck* in Fig. 7 refer to criteria on stress levels, deflection induced by the aerodynamic loads, total weight, SMA material percentage and buckling levels, respectively. A value of 100 indicates full satisfaction of the specific criterion. Picked solutions showed then the best compromise among those different properties. Once the design was fixed, hinges bending rigidities and necessary recovery pre-loads were computed, Table 1. These data represented the main input for the advanced design and manufacture phases, (Stamatelos *et al.* 2012).

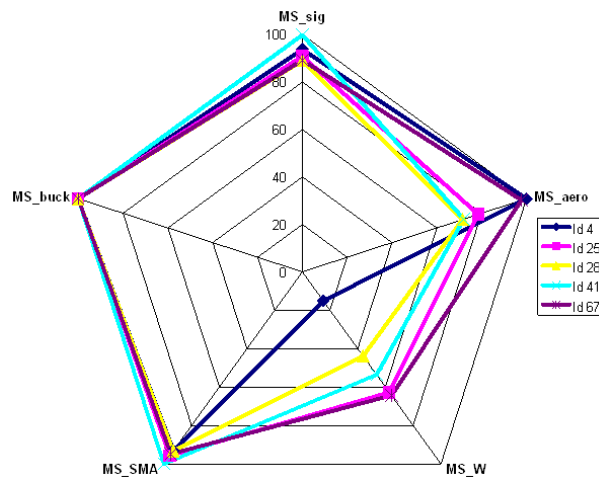


Fig. 7 Radar diagram comparing the different configuration on the basis of the criteria

Table 1 Bending stiffness around the pivots

	Upward elastic el.	Central elastic el.	Downward elastic el.
Bending stiffness [Nm/rad]	767.0	338.6	22.3
Pre-load deflection [deg]	-5.7	-4.7	-4.6
Rotation by aerodynamic loads [deg]	1.0	0.7	0.3
Rotation by the SMA element [deg]	-15.5	-15.6	-15.3

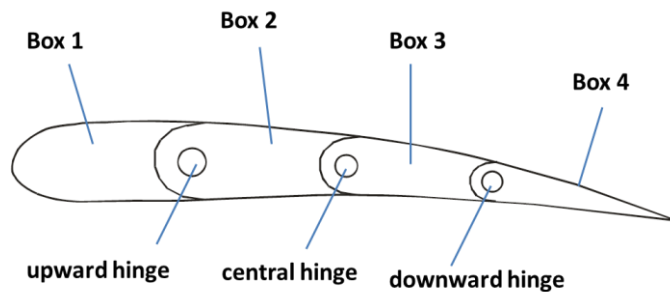


Fig. 8 Reference scheme of the morphing flap

4. Advanced design and manufacture

Having defined the structure, a FE analysis was carried out, to assess constructive details like the span-wise connections among the ribs (spars), the metallic skin integration and the connections among the rib segments. A view of the open model is reported in Fig. 9. The structure ability in withstanding external loads and keeping the target deformed shape was proved through a static analysis. Fig. 9(b) illustrates the flap strained configuration and the related stress field under significant load condition. The main characteristics of the morphing flap are reported in Table 2. The top view of the manufactured flap and a detail of the SMA elements integration are finally illustrated in Fig. 10.



Fig. 9 Flap FE model: internal architecture: non-deformed (a), deformed (b)

5. Experimental campaign

The prototype was tested through a suitable experimental campaign, described in (Chrysochoidis *et al.* (2012), Chrysochoidis *et al.* (2013)).

Dedicated test plans and setups were defined with the aim of collecting accurate information on:

- structure ability in withstanding the most severe operative condition, without any structural damage
- architecture ability to preserve its own (morphed and unmorphed) shape
- structure dynamic behaviour

On the basis of these targets, and considering the static working of the SMA actuators, the campaign was split in two different tasks: one devoted to the static characterization (stress analysis) and to the SMA actuation and the other one to the dynamic behavior of the architecture.

Table 2 Morphing flap main characteristics

REF. BOX ASSY	COMPONENT	MULTIPLICITY	MATERIAL	TOTAL MASS [Kg]
Box 1	rib	3	Al 7075-T6	6.57E-02
	skin (leading edge)	1		7.68E-01
	front spar	1		8.89E-02
1st X cell	SMA – Elastic el.	3	NiTiNol	3.12E-02
	SMA – Actuator el.	3	NiTiNol	3.12E-02
Box 2	Rib	3	Al 7075-T6	2.27E-02
	skin	1		1.43E-01
	second spar	1		6.04E-02
2nd X cell	SMA – Elastic el.	3	NiTiNol	1.51E-02
	SMA – Actuator el.	3	NiTiNol	1.51E-02
Box 3	rib	3	Al 7075-T6	1.03E-02
	skin	1		2.85E-01
	third spar	1		3.58E-02
3rd X cell	SMA – Elastic el.	3	NiTiNol	9.53E-04
	SMA – Actuator el.	3	NiTiNol	9.53E-04
Other components	rib / spar connections	12	Al 7075-T6	2.13E-01
Box 4	rib	4	Al 7075-T6	8.96E-03
	skin	1		3.21E-01
	rear spars	1		3.84E-02
OVERALL FLAP MASS [KG]				2.16
CENTER OF GRAVITY CHORDWISE POSITION [%]				46.4



Fig. 10 Demonstrator top view with accelerometers and excitation point location(a), hinge and SMA wires integration detail (b)

5.1 Static characterization

A dedicated test rig (see Fig. 11) was assembled to allow the integration and the positioning of the DESA prototype in horizontal position.

As shown in Fig. 12 three types of investigations were performed:

- actuation of the prototype through the SMA elements, without any load (functionality tests without loads)
- actuation of the prototype in presence of the most severe operative load condition, to appreciate the SMA ability in approaching to the target shape even in presence of external disturbance;
- application of an additional static load over the most severe one, for stress analysis purpose.



Fig. 11 Demonstrator integrated onto the test rig and pointed by the laser sensor

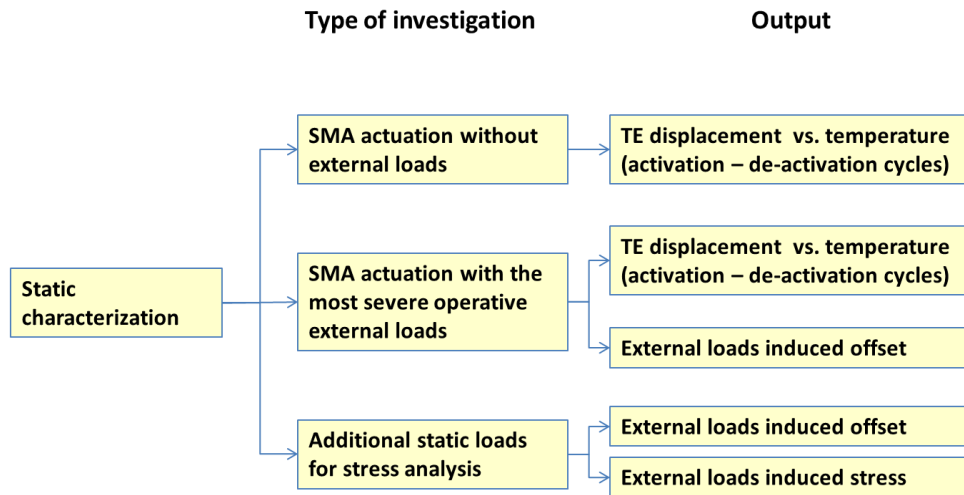


Fig. 12 Static characterization: type of investigation and obtained output

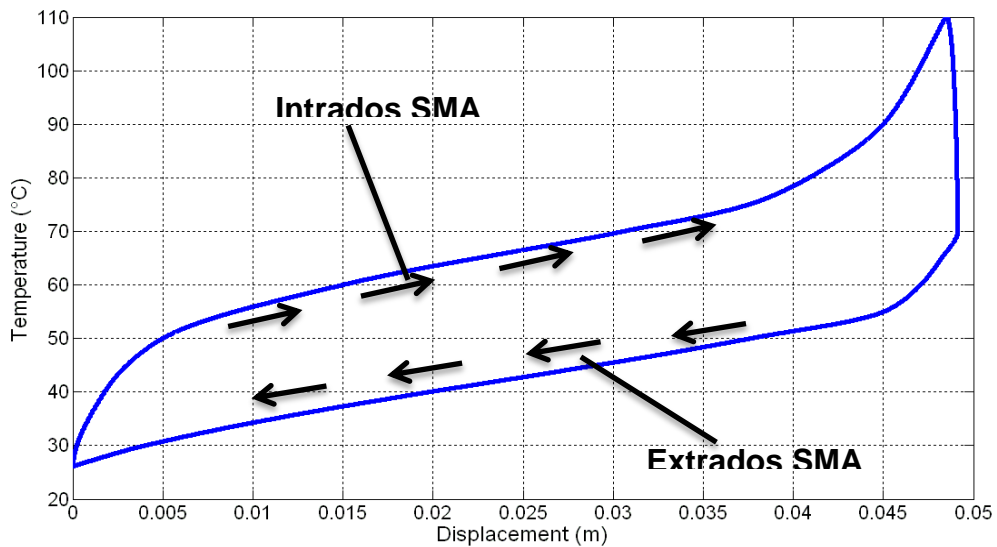


Fig. 13 Trailing edge activation cycle: trailing edge vertical displacement vs. temperature

A power amplifier allowing for current control was used for the activation of the prototype. Resistance electrical insulated wires were wound around the SMA active elements and heated through Joule effect, this way transferring heat to the SMA components.

The displacements along the chord for the different configurations were measured through a Laser Doppler Vibrometer sensor; moreover, on the basis of the numerical stress analysis, the most stressed zones were identified and integrated with strain gage sensors.

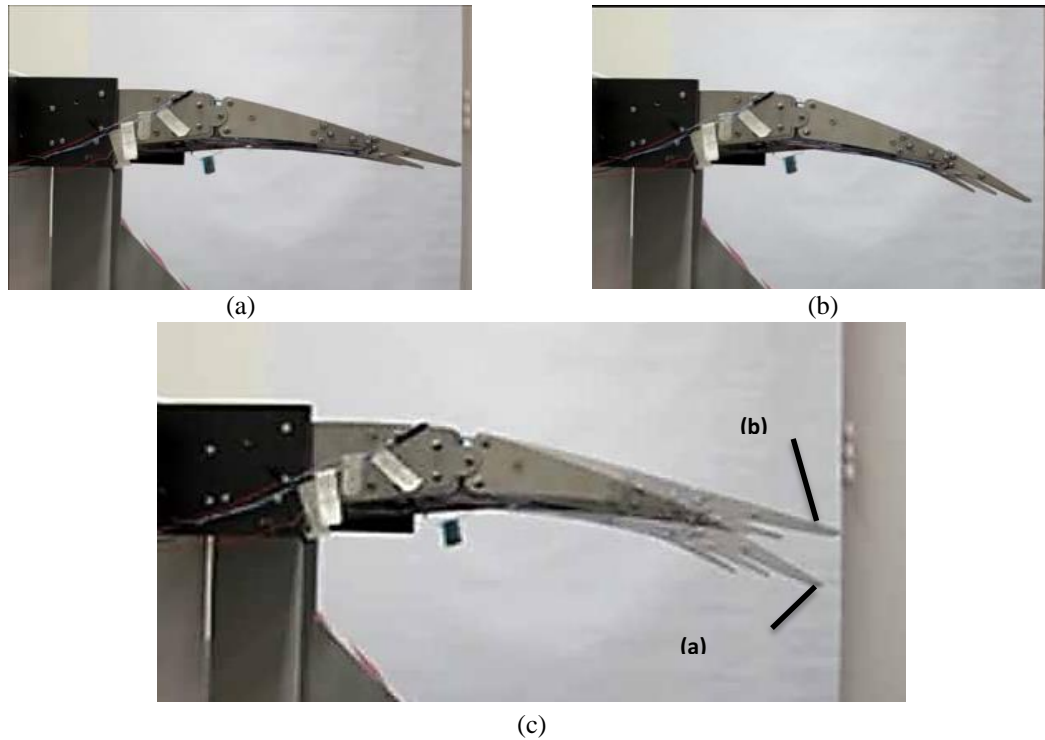


Fig. 14 Unmorphed (a) and morphed flap (b); configuration overlap (c)

During the functionality tests, the SMA elements underwent different heating-cooling cycles to address the necessary training process and to assess the repeatability of performance of the device. A typical activation deactivation cycle is illustrated in Fig. 13, reporting the trailing edge vertical displacement versus the SMA temperature. These cycles were obtained alternatively activating and deactivating the intrados and the extrados SMA elements. The prototype ability to achieve a deflection up to 50 mm at a temperature of 110 °C and then regain its initial configuration was demonstrated. A comparison between the activated and no activated configurations was provided in Fig. 14.

The ability of the prototype to operate under the aerodynamic loads was then investigated. A total weight of 8 kg was distributed along the chord, corresponding to the most severe load condition. The achieved displacement of the trailing edge for an antagonistic activation of the intrados/extrados SMA elements is reported in Fig. 15. A maximum displacement of 65 mm was achieved for a temperature 130°C.

Also the displacements at the different stations of the chord were measured through the Laser sensor on the central rib, obtaining a law well fitted by a parabolic function, as shown in Fig. 16.

These activation tests under load proved that the prototype is able to morph while aerodynamic loads are applied on its surface, contrary to its movement.

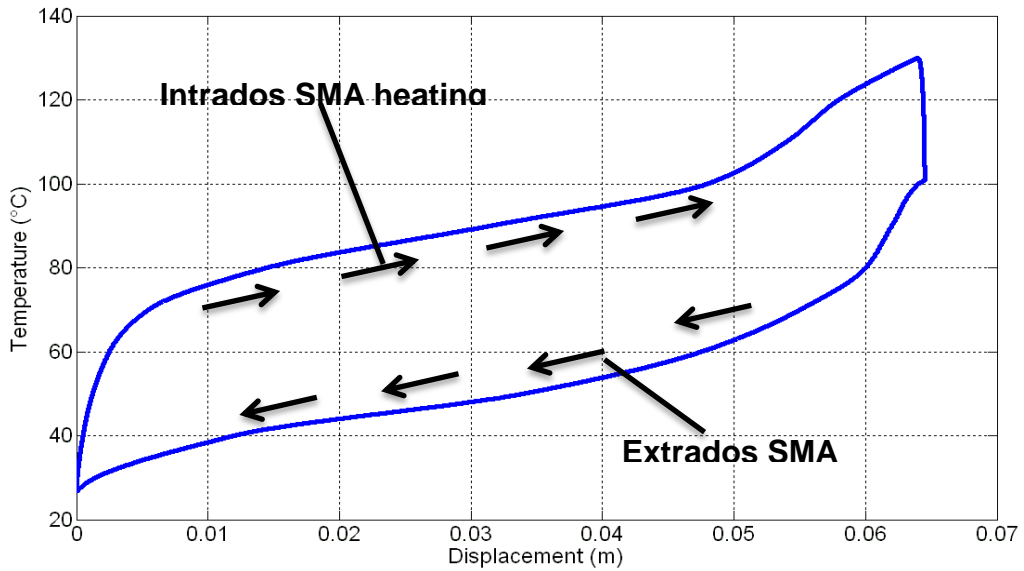


Fig. 15 Trailing edge activation cycle in presence of external loads: trailing edge vertical displacement vs. temperature

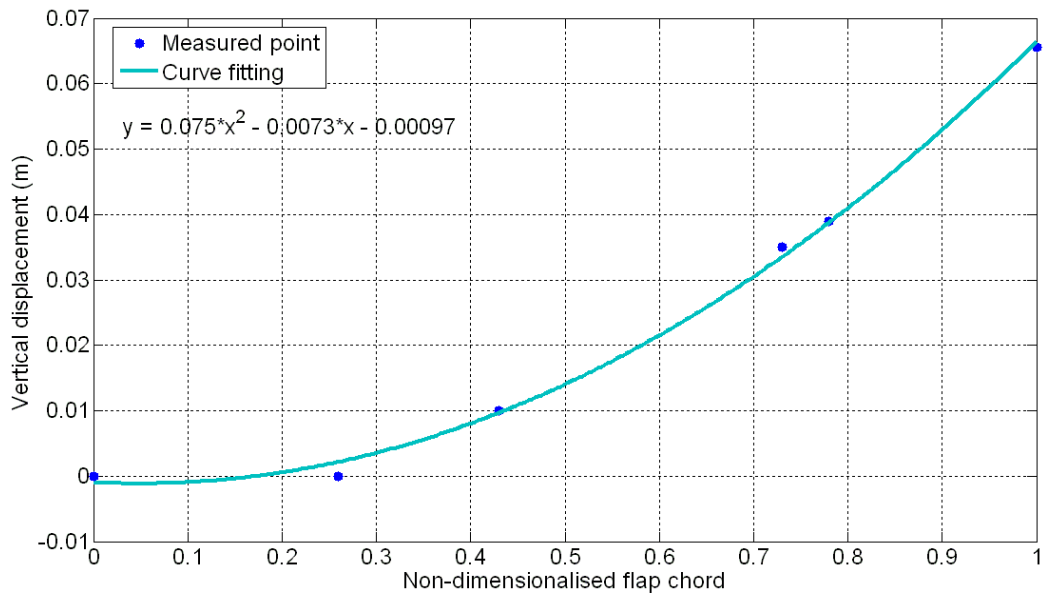


Fig. 16 Flap vertical displacement vs. chord station

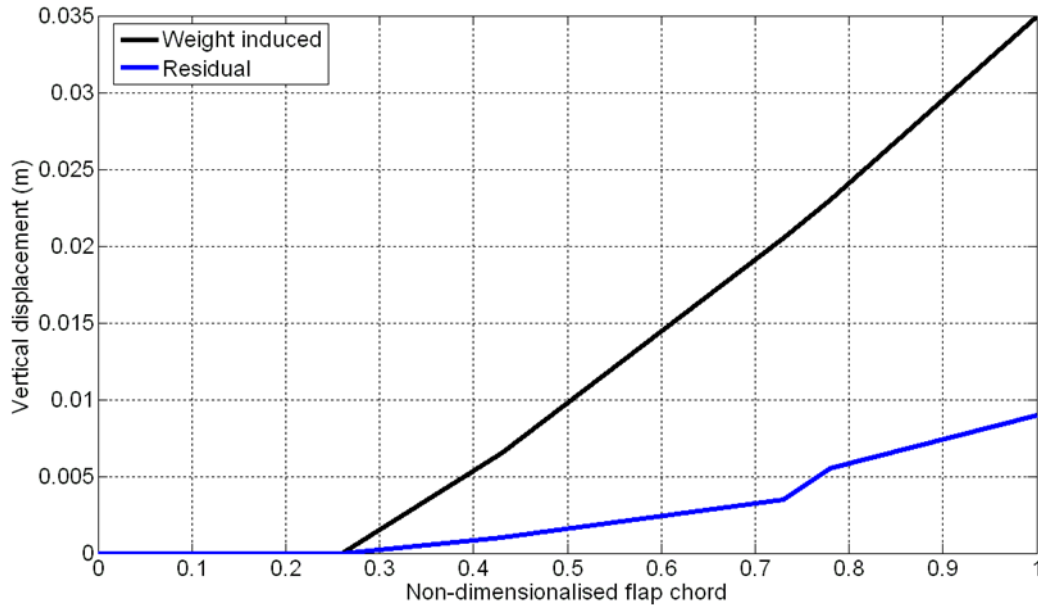


Fig. 17 Weight induced and residual displacements vs. chord station

Also strain measurements were performed through the installed strain gages: no significant strain was recorded to the locations where the strain sensors were attached. These strain measurements also duplicate the design generated strains on the tested loaded structure.

A maximum residual vertical displacement of 9.5 mm was detected with respect to the baseline configuration. As demonstrated by the measured low strain level, this value does not indicate any plasticization of the structure; rather it seems attributable to some gaps and free-play angle.

5.2 Dynamic characterization

The dynamic characterization was carried out for three different constraint conditions:

- cantilevered flap undeformed
- cantilevered flap deformed
- free-free

The extracted modal parameters for the prototype were the modal frequencies, the modal damping and the mode shapes. Only the frequency range between 0 and 80 Hz was investigated. Fig. 10(a) illustrates the prototype during the cantilever characterization as well as the excitation point and the 12 locations where the acceleration was measured.

In Fig. 18 and in Table 3 the 1st modal shape of the 1st mode for the flap in clamped condition, unmorphed and morphed are reported. As evident no appreciable difference were found, showing that the stress field produced by the SMA elements when active does not affect the dynamic of the structure.

Finally the prototype, in free – free conditions, exhibited a torsion mode at a frequency of 17,1 Hz.

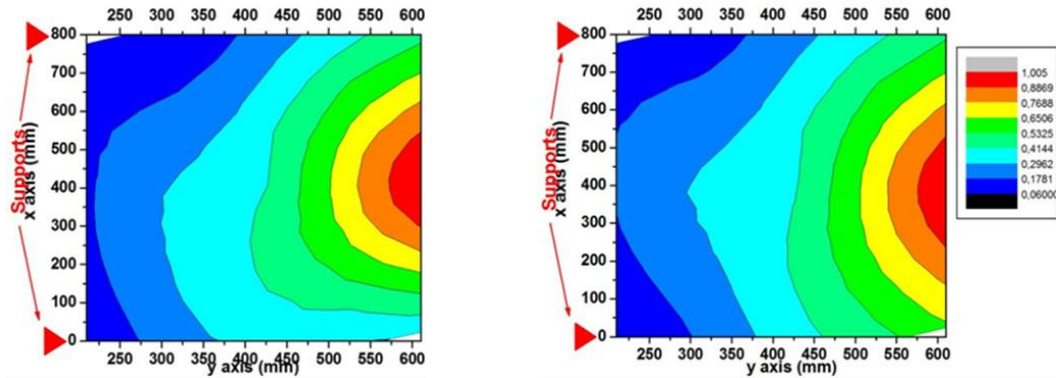
Fig. 18 1st modal shape unmorphed (left) and morphed configurations

Table 3 Main features of the morphing flap

mode no.	configuration	frequency [hz]	modal damping (ζ) [%]
1	Unmorphed	40,6	1,34
1	Morphed	40,7	1.35

6. Conclusions

In the present work, the development of a morphing flap was presented.

The architecture used for the purpose, based on shape memory alloy technology, produces smooth variations of the curvature thus increasing the high lift performance.

Each rib is split into different parts linked each other's by hinges. The relative rotation among these pivots is obtained by 1D SMA elements connecting the rib parts and contacting when activated through Joule effect. The structural rigidity is provided by elastic elements, also assuring the pre-load within the SMA actuator for their complete recovery when no activated. Among the different design solutions, SMA wires used in antagonistic configurations were installed above the hinges, this way taking advantage of the super elastic effect.

A preliminary design phase was performed with the purpose of assessing the main aspects like the number of hinges (i.e., degree of freedom) to approximate the morphed shape, the dimensions of the SMA actuators and the bending stiffness required by the elastic antagonistic elements.

After this phase, the advanced design was carried out, defining the manufacturing details of the prototype, used to validate the numerical predictions.

The experimental campaign included both a static and a dynamic characterization. The static tests proved the structure ability in withstanding the most severe load conditions and in preserving its shape (morphed and unmorphed); furthermore, the functionality tests highlighted the effective capability to produce curvature variations, even larger than the prescribed one. Finally, the dynamic tests showed a similar behavior, in the low bandwidth, of the morphed and unmorphed flap.

Achieved promising results make this architecture worth to be further developed, this way

enhancing its technology readiness level. Future works could focus on a control strategy aimed at assuming intermediate configurations (as for a traditional flap); to this aim it could be thinkable to split the coiling system into different sectors, this way partially activating the SMA; moreover, for the skin an armadillo configuration was adopted, but other solutions can be taken into account like a skin made of zero Poisson modulus material, guaranteeing enough flexibility and, at the same time, a reduced stress level even in morphed configuration.

Acknowledgments

This research was partially funded by the Clean Sky Joint Undertaking under projects GAM-GRA (Grant Agreement for Member- Green Regional Aircraft), related to activities performed within the ITD (Integrated Technology Demonstrator) Green Aircraft.

Furthermore, the authors would like to recall that part of the activity herein presented was developed within a Project Call for Proposal, JTI-CS-2011-1-GRA-02-015, by the Consortium SMyTE.

References

- Ameduri, S., Concilio, A. and Gianvito, A. (2009), "Design of an MR based on device for the adaptive stiffness control of tail shafts", *J. Intel. Mat. Syst. Str.*, **20**(7), 837-848
- Ameduri, S., Concilio, A. and Pecora, R. (2011), "Conceptual design of DESA and SACM based architectures for morphing T/E flap", *GRA-2.2.1-TN-CIRA Plus-TECH-211207 A*, confidential report
- Ameduri, S., Concilio, A. and Pecora, R. (2011), "Desa and sacm concepts comparison", *GRA-2.2.1-TN-Air Green-TECH-201104 B*, confidential report
- Barbarino, S., Ameduri, S. and Pecora, R. (2007), "Wing camber control architectures based on SMA: Numerical investigation", *Proceedings of SPIE of the International Conference on Smart Materials and Nanotechnology in Engineering (SMN2007)*, Harbin, July
- Barbarino S., Pecora R., Lecce L., Concilio A., Ameduri S. and Calvi E. (2009), "A novel sma-based concept for airfoil structural morphing", *J. Mater. Eng. Perform.*, **18**(5), 696-705
- Bil, C., Massey, K. and Abdullah, E. J. (2013), "Wing morphing control with shape memory alloy actuators", *J. Intel. Mat. Syst. Str.*, **24**(7), 879-898
- Brindisi, A., Ameduri, S. and Tiseo, B. (2011), "Preliminary design of wing trailing edge morphing architecture", *GRA 2.2.1 TN CIRA Plus TECH 210105 A*, confidential report
- Clean Sky Joint Undertaking (2011), *Call SP1-JTI-CS-2011-1-GRA-02-015*, http://ec.europa.eu/research/participants/portalplus/static/docs/calls/sp1-jti-cs-2011-01/31103-ct-cs-2011-01-a-15-march_en.pdf
- Chrysochoidis, N., Machairas, T. and Rekatsinas, C. (2012), "D5.1 testing of sacm and desa prototypes", *CleanSky JTI-CS-2011-1-GRA-02-015 D5.1* - confidential report
- Chrysochoidis, N., Machairas, T. and Rekatsinas, C. (2013), "D5.2 test results of sacm and desa prototypes", *CleanSky JTI-CS-2011-1-GRA-02-015 D5.2* - confidential report
- Di Muzio, M. (2010), "Description of nlf wing high-lift-devices", *GRA-2.1.2-DL(D2.1.2-01)-ALA-TECH-209057 A* - confidential report
- Dimino, I. and Concilio, A. (2013), "An adaptive control system for wing te shape control", *Proceedings of the SPIE International Conference on Smart Structures*, San Diego, March
- Grigorie, T.L., Popov, A.V., Botez, R.M., Mamou, M. and Mébarki, Y. (2011), "On-off and proportional-integral controller for a morphing wing. part 1: actuation mechanism and control design", *J. Aerospace Eng.*, **226**(2), 131-145

- Grigorie, T.L., Popov, A.V., Botez, R.M., Mamou, M. and Mébarki, Y. (2011) “On-off and proportional-integral controller for a morphing wing. part 2: control validation – numerical simulations and experimental tests”, *J. Aerospace Eng.*, **226**(2), 146-162
- Guo, S., Li, D. and Liu, Y. (2012), “Multi objective optimization of a composite wing subject to strength and aeroelastic constraints”, *J. Aerospace Eng.*, **226**(9), 1095-1106
- Iannuzzo, G., Riccio, M., Russo, S., Calvi, E., Pecora, R., Lecce, L., Barbarino, S., Concilio, A. and Ameduri, S. (2009), “An actuator device based on a shape memory alloy, and a wing flap assembly fitted with such an actuator device”, Filed on July 21, 2009 at the European Patent Office, patent no. 09165941-7 - 1254
- Inman, D.J. (2011), “Wings: out of the box. determining actuator requirements for controlled morphing air vehicles— aerodynamic loads”, *DARPA Technology Interchange Meeting*, Dayton, November
- Kudva, J.N. (2001), “Overview of the DARPA AFRL Northrop- Grumman smart wing phase 2 program”, *SPIE proceedings of Smart Structures and Materials Conference*, **4332**, Newport Beach, CA, March
- Langbein, S. and Welp, E.G. (2009), “One-module actuators based on partial activation of shape memory components”, *J. Mater. Eng. Perform.*, **18**(5-6), 711-716
- Lesieutre, G.A., Browne, J.A. and Frecker, M.I. (2011), “Scaling of performance, weight, and actuation of a 2-d compliant cellular frame structure for a morphing wing”, *J. Intel. Mat. Syst. Str.*, **22**(10), 979-986
- Maheri, A. and Isikveren, A.T. (2011), “Design of a single-dof kinematic chain using hybrid ga-pattern search and sequential ga”, *J. Mech. Eng. Sci.*, **226**(6), 1633-1643.
- Mcknight, G., Doty, R., Keefe, A., Herrera, G. and Henry, C. (2010), “Segmented reinforcement variable stiffness materials for reconfigurable surfaces”, *J. Intel. Mat. Syst. Str.*, **21**(17), 1783-1793
- Monner, H.P., Bein, Th., Hanselka, H. and Breitbach, E. (1998), “Design aspects of the adaptive wing—the elastic trailing edge and the local spoiler bump”, *Proceedings of the Multidisciplinary Design and Optimization*, London, October.
- Moses, R.W. (1997), “Active vertical tail buffeting alleviation on a twin-tail fighter configuration in a wind tunnel”, *International Forum on Aeroelasticity and Structural Dynamics*, CEAS, June
- Pecora, R., Ameduri, S. and Concilio, A. (2011), “Critical analysis of two designs based on DESA and SACM actuation concepts”, *GRA-2.2.1-TN-Air Green-TECH-210071 A*, confidential report
- Perkins, D.A., Reed, J.L. and Havens, E. (2004), “Morphing wing structures for loitering air vehicles” , *Proceedings of the 45th AIAA/ASME/ASCE/AHS/ASC Structures, Structural Dynamics and Materials Conference*, AIAA, Palm Springs, CA, April
- SADE Project website: http://www.smr.ch/sade/sade_public/home.html
- Schweiger, J., Suleman, A., Kuzmina, S. I. and Chedrik, V.V. (2002), “MDO concepts for an European Research Project on Active Aeroelastic Aircraft”, *Proceedings of the 9th AIAA/ISSMO Symposium on Multidisciplinary Analysis and Optimization*, Atlanta, Georgia, September
- Stamatelos, D., Spathopoulos, T., Karagiannis, T. and Saravanos, D. (2012), “Airfoil morphing based on SMA actuator technology”, *Proceedings of the 7th International Conference Supply on the Wings Aerospace a leading innovator*, Frankfurt, November
- Stanewsky, E. (2001), “Adaptive wing and flow control technology”, *Prog. Aerosp. Sci.*, **37**(7), 583-667